OFFICE OF NAVAL RESEARCH

GRANT: N00014-93-1-0757

R&T CODE 400X119YIP
Dr. Robert J. Nowak

Technical Report No. 5

Electrochemical Deposition of Silver Nanocrystallites on the Atomically Smooth Graphite Basal Plane

by

J. Zoval, R.M. Stiger, P.R. Biernacki, and R.M. Penner*

Prepared for Publication in the

Journal of Physical Chemistry

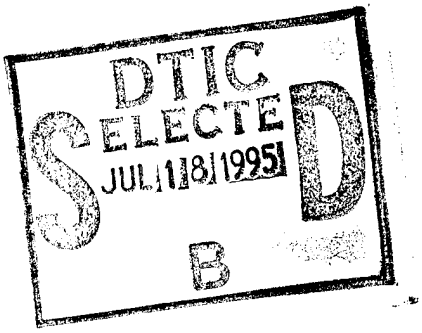

University of California, Irvine
Department of Chemistry
Irvine, CA 92717-2025

June 30, 1995

REPORT DOCUMENTATION PAGE

Form Approved
ONB No. 0704-0188

1. AGENCY USE ONLY (LEAVE BLANK)	2. REPORT DATE	3. REPORT TYPE AND DATES COVERED
	June 30, 1995	Interim May 1994 - June 1995

4. TITLE AND SUBTITLE

Electrochemical Deposition of Silver Nanocrystallites on the Atomically Smooth Graphite Basal Plane

5. FUNDING NUMBERS

N00014-93-1-0757

6. AUTHOR(S)

J. Zoval, R.M. Stiger, P.R. Biernacki, and R.M. Penner*

7. PERFORMING ORGANIZATION NAME(S) AND ADDRESS(ES)

University of California, Irvine
Department of Chemistry
Irvine, CA 92717-2025

8. PERFORMING ORGANIZATION REPORT NUMBER

Technical Report No. 5

9. SPONSOING/MONITORING AGENCY NAME(S) AND ADDRESS(ES)

Office of Naval Research
800 North Quincy Street
Arlington, VA 22217

10. SPONSORING/MONITORING AGENCY REPORT NUMBER

R&T Number:
400X119YIP

11. SUPPLIMENTARY NOTES

12. A. DISTRIBUTION AVAILABILITY STATEMENT

Approved for public release, distribution unlimited

12B. DISTRIBUTION CODE

13. ABSTRACT

A potentiostatic pulse method has been employed to electrochemically deposit silver nanocrystallites on the atomically smooth graphite basal plane surface. Voltage pulses having amplitudes of 100, 250, and 500 mV vs. Ag^o and durations of 10 and 50 ms were applied to graphite surfaces immersed in 1.0 mM aqueous AgF. I vs. t transients recorded during the deposition increased in proportion to $t^{1/2}$ for all depositions. This behavior is diagnostic of an instantaneous nucleation, and three-D growth mode of deposition. Consistent with this model, non-contact atomic force microscopy (NC-AFM) examination of the graphite surface following deposition revealed the existence of silver particles at a coverage of near 10^{10} cm^{-2}. These particles were disk-shaped having a height of 15 to 50Å, and an apparent diameter of 200Å to 600 Å; these dimensions increased smoothly with the coulometric loading.

14. SUBJECT TERMS

Silver, Non-contact atomic force microscopy, nanocrystallites

15. NUMBER OF PAGES

30

16. PRICE CODE

17. SECURITY CLASSIFICATION OF REPORT	18. SECURITY CLASSIFICATION OF THIS PAGE	19. SECURITY CLASSIFICATION OF ABSTRACT	20. LIMITATION OF ABSTRACT
Unclassified	Unclassified	Unclassified	Unlimited

J. Phys. Chem., submitted 6/95

Electrochemical Deposition of Silver Nanocrystallites on the Atomically Smooth Graphite Basal Plane

J. Zoval, R.M. Stiger, P.R. Biernacki, and R.M. Penner*
Institute For Surface and Interface Science
Department of Chemistry
University of California, Irvine
Irvine, CA 92715-2025

Abstract:

A potentiostatic pulse method has been employed to electrochemically deposit silver nanocrystallites on the atomically smooth graphite basal plane surface. Voltage pulses having amplitudes of 100, 250, and 500 mV vs. Ag^0 and durations of 10 and 50 ms to graphite surfaces immersed in dilute (≈1.0 mM) aqueous silver fluoride. Current-time transients recorded during the deposition experiment increased in proportion to time$^{1/2}$ during much of the pulse duration in all deposition experiments. This behavior is diagnostic of an instantaneous nucleation, and three-dimensional growth model of deposition. Consistent with this model, non-contact atomic force microscopy (NC-AFM) examination of the graphite surface following deposition revealed the existence of silver particles at a coverage of near 10^{10} cm^{-2} which were well-separated from one another on atomically smooth regions of the graphite basal plane surface. These particles were disk-shaped having a height of 15Å to 50Å, and an apparent diameter which varied from 200Å to 600 Å; particle dimensions increased smoothly with the coulometric loading over the interval from 0.040 μC cm^{-2} to 40 μC cm^{-2}. Silver nanocrystallites present on the atomically smooth regions of a graphite surface were not be observed using either the scanning tunneling microscope (STM) or conventional repulsive mode atomic force microscope (AFM). In addition to NC-AFM, the characterization of these silver nanocrystallites by transmission electron microscopy lattice imaging, and Auger electron spectroscopy are reported.

*Address correspondence to this author: RMPenner@UCI.edu

Introduction.

Nanometer-scale metal particles possess chemical and physical properties which differ significantly from macroscopic metal phases. In recent years, the list of particle size dependent properties has grown to include bond distances[1-5], the van der Waals attractive force operating between particles[6], the surface plasmon resonance[7-15], the melting point[16,17], the standard electrode potential[18-22], and the photoelectric yield[23-25]. One or more of these properties becomes size-dependent for metal particles having dimensions below a critical threshold which is in the range from 2-10 nm depending on the particular property and metal considered.

Previously, supported metal particles have been obtained by a wide variety of techniques including electric field-assisted deposition of metal aerosols[26,27] , vacuum evaporation of metals[28-30], diffusion-controlled aggregation[c.f.31], inert gas evaporation[c.f.32], e-beam and x-ray nanolithography[33-35], accumulation of colloidal metal particles from solution onto a charged support[36,37], and chemical and electrochemical deposition of metals into nanoscopic templates[38-41].

Electrochemistry has not been employed as a means for preparing large numbers of supported metal nanocrystallites. This fact is surprising when it is considered that nanoscopic metal particles are usually obtained, transiently, when one metal is electrochemically deposited onto the surface of a second at a high over-potential. Indeed, investigations of metal over-potential deposition (OPD) have frequently lead to the observation of metal micro- and nano-crystallites: Harrison and coworkers, for example, observed palladium and silver microcrystallites on electrode surfaces[42-44], and more recently, silver[45] and copper[46-48] nanocrystallites have been observed by *in-situ* scanning tunneling microscopy (STM). The electrochemical preparation of supported metal nanostructures has been closely approached in two recent and novel experiments: Reetz and Helbig[49] have electrochemically formed palladium colloid particles at a platinum electrode surface from solutions of acetonitrile/THF in the presence of tetraalkyl ammonium ions which act as particle stabilizers. The palladium particles synthesized by this method, having diameters in the 1-10 nm range, do not adhere to the platinum surface and are collected instead as a precipitate in the electrochemical cell. Giersig and Mulvaney[50] have accumulated chemically synthesized gold colloid particles on the surfaces of carbon coated grids by electrophoretic deposition. Closest-packed islands of the citrate-stabilized colloid which are one particle monolayer in thickness are thereby obtained.

Several groups have employed scanning probe microscopes to direct the one-at-a-time deposition of supported metal nanoparticles. Li *et al.*[51-53] have developed a

method by which a metal monolayer, present on a platinum STM tip, can be transferred to a nucleation site on a graphite surface to produce a nanoscopic metal particle. Similar tip-directed deposition schemes have been demonstrated by Mandler and coworkers[54], and Kolb and coworkers[55] , whereas LaGraff and Gewirth[56] have employed the tip of an atomic force microscope to direct the growth of nanoscopic copper protrusions on copper surfaces by electrochemical deposition. For practical reasons, the maximum number of metal (or metal oxide[54]) particles accessible by any of these methods is of the order of ten.

In this paper, we report that a potentiostatic pulse method can be employed to electrochemically deposit silver nanocrystallites onto the atomically smooth graphite basal plane. Except for the short durations of our voltage pulses, this procedure is similar to the potentiostatic OPD deposition schemes employed by previous investigators: The potential of a graphite surface immersed in a dilute (1.0 mM Ag^+) silver electrolyte was pulsed to over-potentials of 100-500 mV for durations of either 10 ms or 50 ms. These deposition conditions generated coulometric loadings for silver in the range from 0.040 $\mu C\ cm^{-2}$ to 40 $\mu C\ cm^{-2}$. The topography of the resulting silver deposit was assessed *ex-situ* using non-contact atomic force microscopy (NC-AFM). NC-AFM analysis of the graphite surface revealed the presence of nanoscopic silver particles at a coverage near $10^{10}\ cm^{-2}$. These particles were disk-shaped with average heights in the range from 15-50Å, and apparent diameters which were approximately an order of magnitude larger. Both of these particle dimensions increased smoothly over the accessible range of coulometric loadings. The distributions of these dimensions for silver particles deposited in a particular experiment ranged from 15-30% of the mean. Other important characteristics of the metal particles obtained by this procedure are as follows: 1) Strongly coordinating stabilizers such as citrate and organic thiols, are not involved in the silver particle synthesis; elemental analysis using Auger electron spectroscopy reveals no contaminants, 2) Removal of the silver particles from the graphite surface can be accomplished by ultrasonically agitating a nanocrystallite-modified graphite surface in water, 3) Transmission electron microscopy lattice imaging data reveals that nanoscopic silver particles removed from the graphite electrode surface are crystalline. Because the graphite basal plane surface is electrochemically very inert, and strongly coordinating stabilizers are not involved in the silver electrosynthesis procedure, the graphite-supported silver particles obtained by the potentiostatic pulse method have immediate applications for investigations of the intrinsic electrochemical reactivity of silver particles over a wide range of particle diameters.

Although the mechanism of electrochemical silver OPD on graphite has been investigated previously using scanning tunneling microscopy[45], the existence of nanoscopic silver particles was not discovered in that study presumably because the silver nanocrystallites which nucleate and grow on the atomically smooth graphite basal plane surface are not visible using either the scanning tunneling microscope, or conventional repulsive mode atomic force microscopy (*vide infra*). These silver nanocrystallites interact weakly with the graphite surface and are removed by the sweeping action of the probe tip from the imaging area. Silver micro- and nano-crystallites which nucleate at defect sites, however, *are* observed by STM and AFM and, consequently, it had been concluded[45] that silver OPD on graphite is initiated by nucleation exclusively at defects, such as step edges, on the graphite surface. The NC-AFM data presented here suggests that on low-defect density surfaces such as the graphite basal plane, STM and repulsive mode AFM data can provide a misleading view of nucleation by "ignoring" the presence of weakly adsorbed metal nanocrystallites which are not associated with defects.

Experimental.

The electrochemical deposition of silver on highly oriented pyrolytic graphite basal plane surfaces was performed in a glass and Kel-F cell in which an o-ring exposed a 0.1046 cm^2 circular area of the graphite surface to a N_2-sparged plating solution of aqueous 1.0 mM silver nitrate (Aldrich, 99.999%), 0.10 M potassium nitrate (Fisher >99.95%; twice recrystallized). This solution was prepared using Nanopure water (ρ >18 MΩ). The potentiostatic deposition of silver was accomplished using a silver wire reference electrode immersed directly in the silver plating solution except for silver-free control experiments which were performed using a saturated calomel electrode. A platinum wire counter electrode was employed for all experiments. Silver deposition was effected by stepping the potential of the graphite surface from open circuit, to deposition potentials of -100 mV, -250 mV and -500 mV versus the silver wire and then back to open circuit. The experimental arrangement is shown schematically in Figure 1: An electrolysis pulse from open circuit was generated by gating the working electrode lead of a Bioanalytical Systems CV-27 using a voltage-activated relay. Electrolysis pulses having durations of either 10 ms or 50 ms were generated by closing the relay using square 5.0 V pulses supplied by a Hewlett Packard 33120A arbitrary waveform generator. The current was measured using the ammeter internal to the CV-27, and was recorded using a Nicollet 310 digital storage oscilloscope. The coulometric

loading of silver, Q_{Ag}, was taken to be the charge integrated from the onset of the potentiostatic pulse, uncorrected for double-layer charging.

Non-contact AFM experiments in air were performed using a Park Scientific Instruments (PSI Inc.) AutoProbe cp instrument equipped with the non-contact AFM head. This instrument operates in the slope-detected mode.[57,58] Cantilevers were 2.0 μm thick Ultralevers (PSI Inc.) having a force constant of 18 N/m, a resonance frequency near 300 kHz, and a nominal tip radius of 100Å. The cantilever excitation frequency employed for these measurements was adjusted to be near the maximum slope of the cantilever resonance response curve. A free-space amplitude of cantilever motion (far from the surface) of ≈5Å was employed. This free-space amplitude was damped to ≈1Å during imaging. The piezo tube employed for these investigations was calibrated in the direction perpendicular to the surface using graphite basal plane surfaces on which monoatomic steps were introduced by heating in flowing O_2 in a tube furnace at 650°C for 2-3 minutes. Lateral calibration of the piezo tube was performed by atomic resolution imaging of HOPG, and Au(111). Following electrochemical deposition of silver on a graphite surface, the surface was removed from the plating solution, and rinsed briefly in a stream of Nanopure water. The surface was then allowed to dry in a desiccator prior to examination with the NC-AFM.

Samples suitable for transmission electron microscopy analysis were prepared by dispersing the weakly adsorbed silver particles on carbon coated TEM grids: An aqueous suspension of these particles was first prepared by ultrasonicating a silver particle-modified HOPG surface in ≈200 μl of pure water. The resulting suspension was then deposited on a 3 mm diameter, carbon-coated gold TEM grids (Ted Pella) and the water was evaporated in an oven at 80°C. The samples prepared in this way were examined using either an Akashi model 002B (lattice imaging) or a Zeiss model 10CR (standard bright field imaging). For lattice imaging, an accelerating voltage of 200 keV was employed; for bright field imaging, an accelerating voltage of 100 keV was employed.

Elemental analysis of silver nanostructures was carried out on a Perkin-Elmer model PHI-590 AM scanning Auger microprobe (SAM) with a primary electron energy of 5 KeV.

Results and Discussion.

The potentiostatic deposition of silver nanocrystallites on graphite was accomplished by pulsing the potential of a basal-plane oriented graphite surface from the rest potential of this surface to electrolysis potentials of -100, -250, and -500 mV vs.

$Ag^{o/+}$ for durations of either 10 ms or 50 ms. Representative current-time transients for depositions of 50 ms carried out at these three potentials are shown in Figure 2. Two distinct temporal regimes of interest are readily identified in these transients: At times of less than 5 ms following the application of the potentiostatic pulse, a peaked current-time response is observed for all pulse amplitudes. At longer times from 5 ms to 50 ms, a rising current transient was observed which, at the highest overpotential of 500 mV, was also peaked in most experiments.

Control experiments performed in the absence of silver confirm that the peaked response observed at short times is due to an exponentially decaying double-layer charging current convoluted with the ≈1.0 ms time constant of the potentiostat employed for deposition. In Figure 3, for example, three current-time transients were acquired for the same graphite surface in silver-free 0.1 M potassium nitrate solution. The characteristic peaked current response is clearly evident in these data, and integration of these current peaks (from 0 to 8 ms) yields the linear charge versus pulse amplitude plot shown in the inset of Figure 3. The capacitance obtained from the slope of this line was 1.70 $\mu F\ cm^{-2}$ which is in the normal range for the graphite basal plane surface. In successive silver deposition trials in which the graphite surface was cleaved prior to each experiment, the apparent capacitance of the surface fluctuated by 10-20% presumably due to fluctuations in the defectiveness of the graphite surface which is exposed during cleavage.

The current increase observed at times greater than 5 ms is approximately linear with $time^{1/2}$, as shown in Figure 2B. In previous experiments, a $t^{1/2}$ dependence of the current has been frequently observed[42-44,59-67] for the OPD deposition of metals (including silver) onto inert electrode surfaces such as graphite. It is generally accepted[59,65] that an $I(t) \propto t^{1/2}$ functionality for the deposition current is indicative of an instantaneous nucleation and three-dimensional growth mode of deposition[65]; that is, the growth of a fixed number of silver nuclei by hemispherical diffusive flux. The detailed form of this proportionality, however, has been disputed but Gunawardena *et al.* [59-63]have shown that experimental data for several metals (including silver) is consistent with the expression:

$$I(t) = \frac{zF\pi(2DC^*)^{3/2}M^{1/2}Nt^{1/2}}{\rho^{1/2}} \qquad \text{Eq. (1)}$$

where D is the diffusion coefficient for the soluble form of the metal, C* is the concentration of the metal in solution in units of moles cm^{-3}, M is the atomic weight of the metal (or the formula weight of soluble metal complex), N is the total number of metal nuclei present on the electrode surface, and ρ is the density of the metal.

Using Eq. (1), and the known diffusion coefficient for Ag^+ ($D_{Ag+} = 1.0 \times 10^{-5}$ cm^2 s^{-1})[61], the value of N can be estimated from the slope of linear I(t) versus $t^{1/2}$ plots such as those shown in Figure 2B. For the three plots shown, the calculated N values are: 2.7×10^9 (500 mV), 4.3×10^8 (250 mV), and 4.2×10^7 (100 mV). These N values can be compared directly with the areal density of silver nuclei estimated from NC-AFM images of the graphite electrode surface (*vide infra*).

In our initial efforts to characterize these silver deposits using scanning probe microscopy, STM and conventional repulsive mode AFM were employed. However we were consistently unable to obtain high quality, low noise, images using either of these techniques. Using either the AFM (and applied forces as small as 0.1 nN) or STM (with tunneling currents of ≈0.1 nA and biases in the range from 20 mV - 1.0V), line scans typically exhibited an unusually high level of noise. This noise was not reproduced in adjacent line scans to any appreciable extent, and was not diminished by the adjustment of parameters such as the applied force, the tunneling current set point, the imaging bias, or the fast-scan frequency. Topographic features of the graphite surface such as step edges, however, were readily identifiable from these images (indicating that the image window of the microscope was not subject to unusual instability), and an accumulation of debris which was presumed to be deposited silver was visible on these defects, however isolated silver nuclei were never observed on atomically smooth regions of the graphite surface in any of these experiments. Because of the unusually low quality of these image data, they are not included here.

Non-contact atomic force microscopy (NC-AFM) was employed in an attempt to overcome the noise problems inherent to the STM and repulsive mode AFM experiments. Like the conventional repulsive mode AFM, the operational principle of the NC-AFM (also called the "dynamic", "attractive mode", and "ac" atomic force microscope) involves the detection and maintenance of a small force which is exerted locally on the probe tip by the sample surface. In the NC-AFM experiment, however, the probe tip is located in the *attractive* region of the tip-sample interaction potential and at greater distances from the surface of 10-15Å. The attractive tip-sample forces present in this separation regime are smaller than those involved in repulsive mode AFM imaging (10^{-11}-10^{-12} N vs. 10^{-9}N), with the result that the silicon NC-AFM tip is a less perturbative probe of the surface structure. The attractive force imparted to the tip is

detected optically as a deflection of a stiff (18 N/m) silicon AFM cantilever toward the sample surface. As compared with repulsive mode AFM, the smaller forces coupled with greater cantilever stiffness necessitate a more sensitive detection scheme for the NC-AFM instrument: Cantilever displacements are detected using either of two schemes in which the cantilever (or sample) is dithered near its resonance frequency with an amplitude of ≈1.0Å, and force gradients are detected by measuring either the amplitude ("slope" detection) or phase of the cantilever vibration. The PSI instrument employed here utilized the slope detection principle. Previous work has established that NC-AFM is superior to STM or repulsive mode AFM for the investigation many compliant surfaces[58,68,69] and for observing weakly adsorbed or laterally mobile molecular species.[70].

In Figure 4 are shown NC-AFM images for three graphite surfaces following the deposition of silver. Coulometric loadings, Q_{Ag}, of 0.564 μC cm^{-2} (Fig.4A,B), 7.59 μC cm^{-2} (Fig.4C,D), and 15.7 μC cm^{-2} (Fig.4E,F) are represented, and for each, NC-AFM images at two magnifications are shown. The prominent topographic feature present for all three surfaces are circular protrusions, having diameters of ≈300Å in Fig. 4A to ≈600Å in Fig. 4C, which are present at an areal density of ≈0.3-1.2 x 10^{10} cm^{-2}. The heights of these protrusions, which are evident from the line scans shown in Figure 5A, increase with Q_{Ag} from 20Å (Fig. 4A) to about 40Å (Fig. 4C). Increases in the apparent diameter of these silver particles with Q_{Ag} are also evident (Figure 5B), however, the apparent diameters obtained from NC-AFM image data are exaggerated by convolution with the geometry of the silicon probe tip which has an ultimate radius of approximately 100Å. Since several different silicon probe tips were employed for these measurements, and the exact dimensions of each are unknown, it is impossible to deconvolve the tip contribution from the NC-AFM image data. Transmission electron microscopy (TEM) data for several samples in which the deposited silver particles were removed from the graphite surface (discussed in greater detail below) suggest that the apparent particle diameter is larger than the true particle diameter by about twice the nominal 100Å tip radius or 200Å; approximately as expected.

Elemental analysis of these surfaces using a scanning Auger microprobe (SAM) instrument yielded spectra like that shown in Figure 6. Except for carbon, only argon - a contaminant of the instrument - is present at detectable levels in addition to silver on these surfaces. It was sometimes possible to dislodge silver nanocrystallites by ultrasonication of a graphite surface in 500 μl of pure water for several minutes following silver particle deposition. The resulting suspension of particles was then drop-coated onto a carbon-coated gold TEM grid, and oven dried at 80°C for several minutes. High

resolution TEM inspection of particles transferred in this way frequently yielded images like that shown in Figure 7. In this image lattice fringes are visible for two ≈100Å diameter silver particles. For both of the nanocrystallites shown here, the lattice spacing obtained from the image equals 2.37 Å which corresponds to the distance along the [111] direction separating (111) planes of atoms for face-centered cubic silver. When combined with the electrochemical data presented above, the SAM and TEM data allow identification of the protrusions observed in Figure 4 as silver nanocrystallites resulting from the potentiostatic reduction of silver at the graphite surface.

For control experiments in which only silver was deleted from the plating solution (as for example in the experiments of Figure 3), it was always possible locate regions of the graphite surface where NC-AFM imaging revealed a low areal density of particles similar to those shown in Figure 4. A low coverage of particles was also observed upon exposure of the graphite surface to the silver plating solution (and subsequent rinsing of the surface with water) when a potentiostatic pulse was not applied. These protrusions are attributed to contaminants of the Nanopure water and the supporting electrolyte employed in the deposition. The areal density of contaminant particles, however, was always very much lower than for potentiostatically deposited samples like those imaged in Figure 4: In all the control experiments carried out (> 30 surfaces and hundreds of NC-AFM images), the largest number of contaminant particle encountered in a single 1.0 μm^2 image was four. On average, NC-AFM images of control surfaces yielded 1 particle per 1.0 μm^2 image window corresponding to an areal density of contaminating particles equal to 1.0×10^8 cm^{-2}.

In Figure 8, histograms of the particle height (Fig. 8A) and apparent particle diameter (Fig. 8B), measured from NC-AFM images, are shown for a series of four potentiostatic depositions which generated Q_{Ag} values from 0.040 to 2.80 μC cm^{-2}. The standard deviations of these distributions vary from 16% of the mean (for both height and diameter) for the Q_{Ag} = 0.071 μC cm^{-2} sample to 30% (height) and 24% (diameter) for the 1.67 μC cm^{-2} sample. In general, the monodispersity measured in this way was better for smaller Q_{Ag}. No attempt has as yet been made to optimize the deposition parameters to improve on the particle monodispersity, and it is very possible that adjustments to the deposition conditions will lead to substantially narrow distributions. At present, this is an area of on-going interest.

It is useful to compare the predictions of Equation (1) with the NC-AFM data of Figure 4 in terms of the areal density of silver particles. As already noted, equation (1) permits the total number of electrochemically active silver nuclei, N, to be extracted from the slopes of the I versus $t^{1/2}$ plots shown in Figure 2B. For the three transients shown in

Figure 2A, the predicted N values can be divided by the electrode area of 0.1046 cm^2 to yield areal number densities of 2.6 x 10^{-10} cm^{-2} (500 mV), 4.2 x 10^{-9} cm^{-2} (250 mV), and 4.1 x 10^{-8} cm^{-2} (100 mV). The first two of these values bracket the range of areal densities we typically observe in the NC-AFM data like that shown in Figure 4 (i.e., 0.3-1.2 x 10^{10} cm^{-2}) for surfaces prepared at all three overpotentials, whereas the prediction based on the 100 mV overpotential transients is too small by about an order of magnitude. The origin of this disparity is not immediately clear, however, the experimentally observed invariance of the particle areal density with overpotential facilitates a direct comparison of the particle heights for silver particle (deposited at all three overpotentials), as a function of Q_{Ag}. This comparison is provided by the plot shown in Figure 9. Provided the total number of silver particles, N, is constant, the height (or radius), r, of N identical hemispherical silver particles should be proportional to $Q_{Ag}^{1/3}$ and given by the equation:

$$r = \left[\frac{3}{2}\frac{M}{z\pi F\rho N}\right]^{1/3} Q_{Ag}^{1/3} \qquad \text{Eq. (2)}$$

The solid line shown in Figure 2 is a fit of Eq. (2) to the experimental data using a value for the parameter N of 8.7 x 10^9 total particles, corresponding to 8.3 x 10^{10} cm^{-2}. The agreement obtained is reasonable except for Q_{Ag} values greater than ≈15 μC cm^{-2}, and the value of N employed is within an order of magnitude of the experimentally measured values. The deviation of the high Q_{Ag} data from this $Q_{Ag}^{1/3}$ dependence is real, however, and it is useful to attempt to understand the origin of this deviation.

The most likely origin for this negative deviation for high Q_{Ag} data from Eq. (2) is apparent in the NC-AFM image of Figure 4F: A number of distinctly larger silver particles having diameters of 1000-5000Å and heights of several hundred angstroms are clearly visible in the NC-AFM image of this electrode for which Q_{Ag} = 15 μC cm^{-2}. For graphite surfaces treated with smaller Q_{Ag} , these "micron-scale" crystallites were seldom observed. As the Q_{Ag} was increased above 15 μC cm^{-2}, further growth in the dimensions of the *nanoscopic* silver particles was significantly retarded. Instead, the number and size of *micron-scale* crystallites was observed to dramatically increase. The presence of these micron-scale particles was particularly easy to monitor since they are readily visibly by dark-field optical microscopy. The emergence of micron-scale silver crystallites provides a clear origin for the negative deviation evident in Figure 9: At values of Q_{Ag} greater than ≈15 μC cm^{-2}, a branching occurs in which an ever increasing

fraction of the deposition charge is consumed with the deposition of silver onto micron-scale crystallites instead of onto nanocrystallites on the surface. The extent of this branching behavior was so pronounced that silver nanocrystallites which were indistinguishable from those shown in Figure 4F, could readily be observed - coexisting with a high coverage of silver microcrystallites - on graphite surfaces having extremely high silver loadings of $Q_{Ag} > 100$ mC cm^{-2}. Since this coulometric loading is in line with the Q_{Ag} values employed in many earlier investigations of OPD silver deposition, it is likely that silver nanocrystallites have been present on the electrode surfaces in many of these studies[42,43,45,61] From the data presented here, it is absolutely clear that nanoscopic silver particles play an integral role in the silver deposition mechanism at low coverages, and may be important in the evolution of the silver deposit at higher coverages, however the existence of these nanoscopic particles on the electrode surface has gone undetected until now.

Summary

A potentiostatic pulse electrochemical method has been employed to deposit silver nanocrystallites onto the atomically smooth graphite basal plane surface. Because of the crystallinity of these particles and the absence of strongly coordinating stabilizers in the synthesis procedure, these silver nanocrystallites are ideal candidates for the investigation of a variety of metal particle size-dependent phenomena.

It is particularly important to recognize the fundamental similarity of the experiment described here to previous OPD deposition experiments, including those in which STM was employed to characterize the electrode topography. This implies that nanoscopic metal particles have been present but undetected in this previous work, and cautions against the use of STM or repulsive mode AFM to characterize the very early stages of electrochemical nucleation and growth of metals.

Acknowledgment

The financial support of this work was provided by grants from the National Science Foundation (#DMR-9257000), the Office of Naval Research (#400X119YIP). RMP also acknowledges financial support as an A.P. Sloan Foundation Fellow, a Camille Dreyfus Teacher-Scholar, and an Arnold and Mabel Beckman Foundation Young Investigator. The authors express their gratitude to Mr. Art Moore of Advanced Ceramics Inc. for the donation of some of the graphite employed for these investigations, and to Park Scientific Instruments for the donation of some of the Ultralevers employed

for the NC-AFM imaging experiments. Valuable discussions with Dr. Ralph Nyffenegger are also gratefully acknowledged.

Literature Cited

1. P.A. Montano, H. Purdum, G.K. Shenoy, T.I. Morrison and W. Schulze, *Surf. Sci.,* **156** (1985) 228.
2. P.A. Montano, W. Schulze, B. Tesche, G.K. Shenoy and T.I. Morrison, *Phys. Rev. B,* **30** (1984) 672.
3. G. Apai, J.F. Hamilton, J. Stohr and A. Thompson, *Phys. Rev. Lett.,* **43** (1979) 165.
4. C. Solliard and M. Flüeli, *Surf. Sci.,* **156** (1985) 487.
5. H.J. Wasserman and J.S. Vermaak, *Surf. Sci.,* **22** (1970) 164.
6. H. Burtscher and A. Schmidt-Ott, *Phys. Rev. Lett.,* **48** (1982) 1734.
7. L. Genzel, T.P. Martin and U. Kreibig, *Z. Physik. B,* **21** (1975) 339.
8. J.R. Heath, *Phys. Rev. B,* **40** (1989) 9982.
9. R.H. Doremus, *J. Chem. Phys.,* **40** (1964) 2389.
10. H. Doremus, *J. Chem. Phys.,* **42** (1965) 414.
11. M.A. Smithard, *Sol. State. Commun.,* **14** (1974) 407.
12. R. Dupree and M.A. Smithard, *J. Phys. C,* **5** (1972) 408.
13. U. Kreibig and L. Genzel, *Surf. Sci.,* **156** (1985) 678.
14. T. Schimmel, H.-G. Bingler, D. Franzke and A. Wokaun, *Adv. Mat.,* **6** (1994) 303.
15. J.L. Coffer, J.R. Shapley and H.G. Drickamer, *J. Am. Chem. Soc.,* **112** (1990) 3736.
16. P. Buffat and J.-P. Borel, *Phys. Rev. A,* **13** (1976) 2287.
17. T. Castro, R. Reifenberger, E. Choi and R.P. Andres, *Phys. Rev. B,* **42** (1990) 8548.
18. W.J. Plieth, *Surf. Sci.,* **156** (1985) 530.
19. W.J. Plieth, *J. Phys. Chem.,* **86** (1982) 3166.
20. A. Henglein, *Topics in Current Chemistry,* **141** (1988) 113.
21. A. Henglein, *Chem. Rev.,* **89** (1989) 1861.
22. A. Henglein, *J. Phys. Chem.,* **97** (1993) 5457.
23. U. Müller, A. Schmidt-Ott and H. Burtscher, *Z. Phys. B,* **73** (1988) 103.
24. A. Schmidt-Ott, P. Schurtenberger and H.C. Siegmann, *Phys. Rev. Lett.,* **45** (1980) 1284.
25. B. Schleicher, H. Burtscher and H.C. Siegmann, *Appl. Phys. Lett.,* **63** (1993) 1191.
26. K. Deppert, I. Maximov, L. Samuelson, H.-C. Hansson and A. Wiedensohler, *Appl. Phys. Lett.,* **64** (1994) 3293.
27. T. Junno, S. Anand, K. Deppert, L. Montelius and L. Samuelson, *Appl. Phys. Lett.,* **66** (1995) 3295.
28. T.A. Dorling, B.W.T. Lynch and R.L. Moss, *J. Catal.,* **20** (1971) 190.
29. S. Ladas, R.A. Dalla Betta and M. Boudart, *J. Catal.,* **53** (1978) 356.

30. T. Uchijima, J.M. Merrman, Y. Inoue, R.L. Burwell, D. Butt and J.B. Cohen, *J. Catal.,* **50** (1977) 464.
31. H. Röder, E. Hahn, H. Brune, J.-P. Bucher and K. Kern, *Nature,* **366** (1993) 141.
32. C.G. Granqvist and R.A. Buhrman, *J. Appl. Phys.,* **47** (1976) 2200.
33. P.E. Schmidt, M. Kosemura, M. Okada and N. Yokoyama, *J. Vac. Sci. Technol. B,* **9** (1991) 1598.
34. H.I. Liu, N.I. Maluf, R.F.W. Pease, D.K. Biegelsen, N.M. Johnson and F.A. Ponce, *J. Vac. Sci. Technol. B,* **10** (1992) 2846.
35. I. Zuburtikudis and H. Saltsburg, *Science,* **258** (1992) 1337.
36. R.G. Freeman and e. al., *Science,* **267** (1995) 1629.
37. K.C. Grabar, R.G. Freeman, M.B. Hommer and M.J. Natan, *Anal. Chem.,* **34** (1995) 735.
38. X. Bo and L. Kevan, *J. Phys. Chem.,* **95** (1991) 1147.
39. C.A. Foss, M.J. Tierney and C.R. Martin, *J. Phys. Chem.,* **96** (1992) 9001.
40. C.A. Foss, G.L. Hornyak, J.A. Stockert and C.R. Martin, *J. Phys. Chem.,* **98** (1994) 2963.
41. B. Xu and L. Kevan, *J. Phys. Chem.,* **96** (1992) 2642.
42. J.A. Harrison, *J. Electroanal. Chem.,* **36** (1972) 71.
43. D.J. Astley, J.A. Harrison and H.R. Thirsk, *Trans. Faraday. Soc.,* **62** (1968) 192.
44. M.F. Bell and J.A. Harrison, *J. Electroanal. Chem.,* **41** (1973) 15.
45. L. Vazquez, C.A. Hernandez, P. Carro, P. Ocon, P. Herrasti, C. Palacia, J.M. Vara, R.C. Salvarezza and A.J. Arvia, *J. Phys. Chem.,* **96** (1992) 10454.
46. R.J. Nichols, W. Beckmann, H. Meyer, N. Batina and D.M. Kolb, *J. Electroanal. CHem.,* **330** (1992) 381.
47. R.J. Nichols, D.M. Kolb and R.J. Behm, *J. Electroanal. CHem.,* **313** (1991) 109.
48. N. Batina, D.M. Kolb and R.J. Nichols, *Langmuir,* **8** (1992) 2572.
49. M.T. Reetz and W. Helbig, *J. Am. Chem. Soc.,* **116** (1994) 7401.
50. M. Giersig and P. Mulvaney, *Langmuir,* **9** (1993) 3408.
51. *Nanoscale Probes of the Solid-Liquid Interface*; W. Li, T. Duong, J.A. Virtanen and R.M. Penner, Ed.; Kluwer Academic Publishers: Netherlands, 1995, pp 183.
52. W. Li, J.A. Virtanen and R.M. Penner, *Appl. Phys. Lett.,* **60** (1992) 1181.
53. W. Li, J.A. Virtanen and R.M. Penner, *J. Phys. Chem.,* **96** (1992) 6529.
54. I. Shohat and D. Mandler, *J. Electrochem. Soc.,* **141** (1994) 995.
55. R. Ullman, T. Will and D.M. Kolb, *Chem. Phys. Lett.,* **209** (1993) 238.
56. J.R. Lagraff and A.A. Gewirth, *J. Phys. Chem.,* **98** (1994) 12246.
57. T.R. Albrecht, P. Grütter, D. Horne and D. Rugar, *J. Appl. Phys.,* **69** (1991) 668.

58. R. Lüthi, E. Meyer, L. Howald, H. Haefke, D. Anselmetty, M. Dreier, M. Rüetschi, T. Bonner, R.M. Overnewy, J. Frommer and H.-J. Güntherodt, *J. Vac. Sci. Technol. B,* **12** (1994) 1673.
59. G. Gunawardena, G. Hills, I. Montenegro and B. Scharifker, *J. Electoanal. Chem.,* **138** (1982) 225.
60. G. Gunawardena, G. Hills, I. Montenegro and B. Scharifker, *J. Electroanal. Chem.,* **138** (1982) 255.
61. G. Gunawardena, G. Hills and I. Montenegro, *J. Electroanal. CHem.,* **138** (1982) 241.
62. G. Gunawardena, G. Hills and I. Montenegro, *J. Electroanal. Chem.,* **184** (1985) 357.
63. G. Gunawardena, G. Hills and I. Montenegro, *J. Electroanal. Chem.,* **184** (1985) 371.
64. G.A. Gunawardena, G.J. Hills and I. Montenegro, *Electrochimica Acta,* **23** (1978) 693.
65. *The Fundamentals of Metal Deposition*; J.A. Harrison and H.R. Thirsk, Ed.; Marcel Dekker: New York, 1971; Vol. 5.
66. W. Davison and J.A. Harrison, *J. Electroanal. Chem.,* **44** (1973) 213.
67. B. Scharifker and G. Hills, *J. Electroanal. CHem.,* **130** (1981) 81.
68. R. Giles, J.P. Cleveland, S. Manne, P.K. Hansma, B. Drake, P. Maivald, C. Boles, J. Gurley and V. Elings, *Appl. Phys. Lett.,* **63** (1993) 617.
69. D. Anselmetti, M. Dreier, R. Lüthi, T. Richmond, E. Meyer, J. Frommer and H.-J. Güntherodt, *J. Vac. Sci. Technol. B,* **12** (1994) 1500.
70. T.M. McIntire, R.M. Penner and D. Brant, *Macromol.,* **in press** (1995)

Figure Captions

Figure 1. Schematic diagram of the instrument employed for pulsed potentiostatic deposition of silver nanocrystallites.

Figure 2. A. Current-time transients for three pulsed potentiostatic deposition experiments at basal-plane oriented pyrolytic graphite surfaces, with pulse amplitudes as indicated, and pulse durations of 50 ms. The deposition solution was aqueous 1.0 mM silver nitrate, 0.10 M potassium nitrate.
B. Plots of current versus time$^{1/2}$ for the three transients shown in A.

Figure 3. Current-time transients for aqueous 0.10 M potassium nitrate in the absence of silver. Pulse durations were 50 ms, and pulse amplitudes are as shown.
Inset - Plot of the integrated charge for the first 8 msec of each pulse versus the pulse amplitude.

Figure 4. Non-contact atomic force micrographs of three basal plane-oriented graphite surfaces following the deposition of silver using the potentiostatic pulse method. Three different conditions of pulse amplitude, pulse duration, and coulometric loading are shown; each at two different magnifications:
A,B. The deposition voltage was -250 mV, and the pulse duration was 10 ms. Q_{dep} = 0.564 $\mu C\ cm^{-2}$.
C,D. The deposition voltage was -250 mV, and the pulse duration was 50 ms. Q_{dep} = 7.59 $\mu C\ cm^{-2}$.
E,F. The deposition voltage was -500 mV, and the pulse duration was 50 ms. Q_{dep} = 15.7 $\mu C\ cm^{-2}$.

Figure 5. Line-scans taken from the $\approx$1.0 μm^2 NC-AFM images of Figure 4A, C, and E, showing a cross-sectional view of the silver particles on these surfaces.

Figure 6. Representative scanning Auger microprobe elemental analysis of a graphite surface following the deposition of silver nanocrystallites using the potentiostatic pulse method.

Figure 7. Transmission electron microscopy lattice imaging micrograph of nanoscopic silver particles after removal of these particles from a graphite surface.

Figure 8. Histograms of the particle height (A) and the apparent particle diameter (B) for four graphite surfaces following the deposition of silver by potentiostatic pulse. The preparation conditions for the four sample shown are as follows:

(a) Pulse duration = 10 ms, pulse amplitude = 100 mv, $Q_{dep} = 0.040\ \mu C\ cm^{-2}$.

(b) Pulse duration = 10 ms, pulse amplitude = 250 mV, $Q_{dep} = 0.071\ \mu C\ cm^{-2}$.

(c) Pulse duration = 50 ms, pulse amplitude = 500 mV, $Q_{dep} = 1.67\ \mu C\ cm^{-2}$.

(d) Pulse duration = 50 ms, pulse amplitude =500 mV, $Q_{dep} = 2.80\ \mu C\ cm^{-2}$.

Figure 9. Plot of particle height (measured from NC-AFM image data) versus Q_{dep} for graphite surfaces on which silver nanocrystallites had been deposited by potentiostatic pulse. Circular data points (○) indicate potentiostatic pulse experiments in which the pulse duration was 10 ms; square data points (□) indicate the pulse duration was 50 ms; the pulse amplitude is indicated by each data point in this plot.

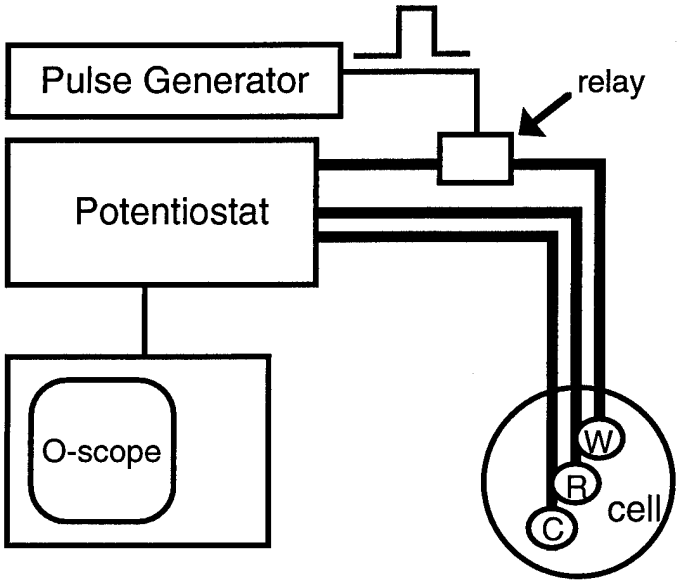

Figure 1. Zoval *et al.*, **UCI Chemistry**

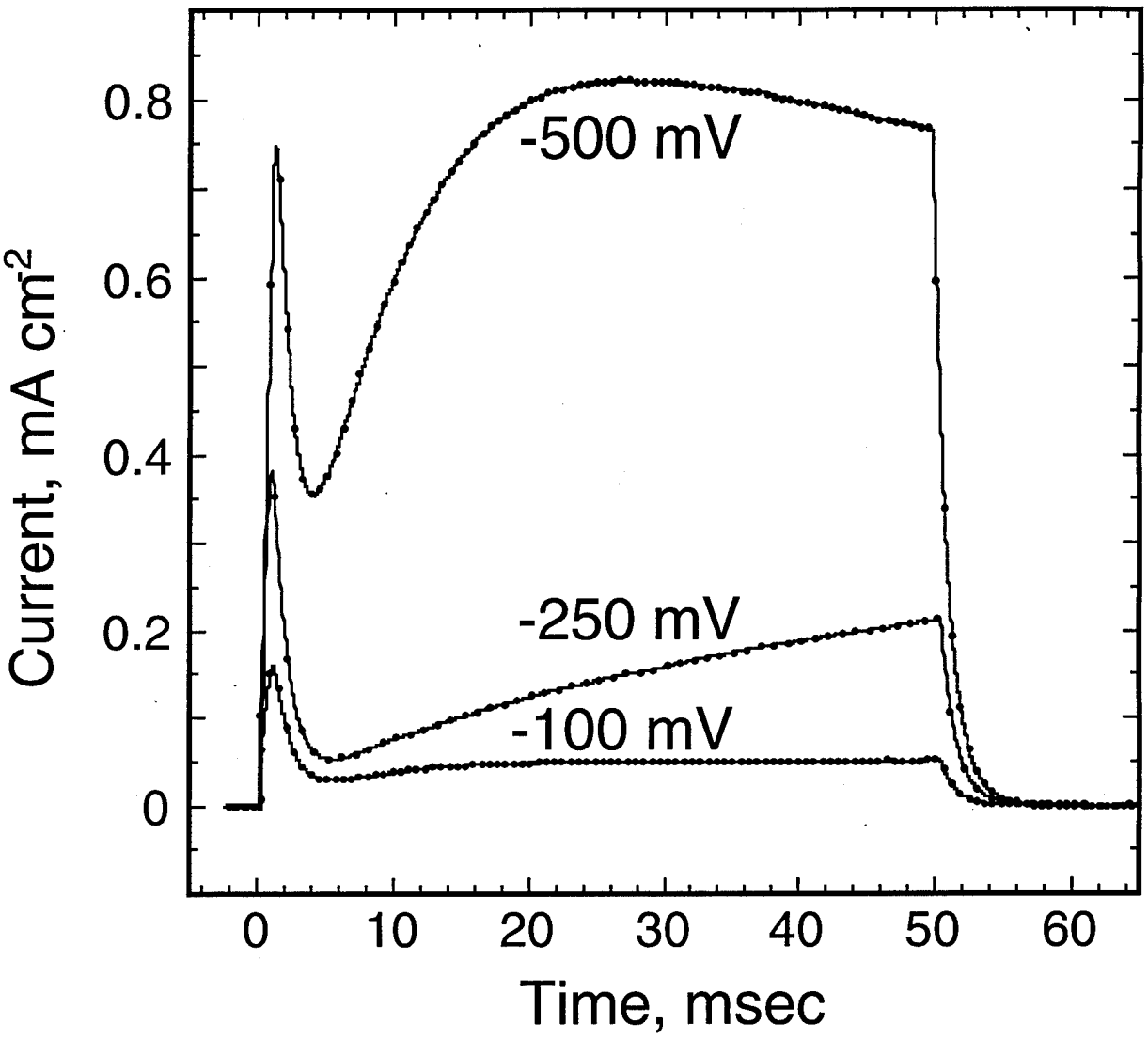

Figure 2A. Zoval *et al.*, **UCI Chemistry**

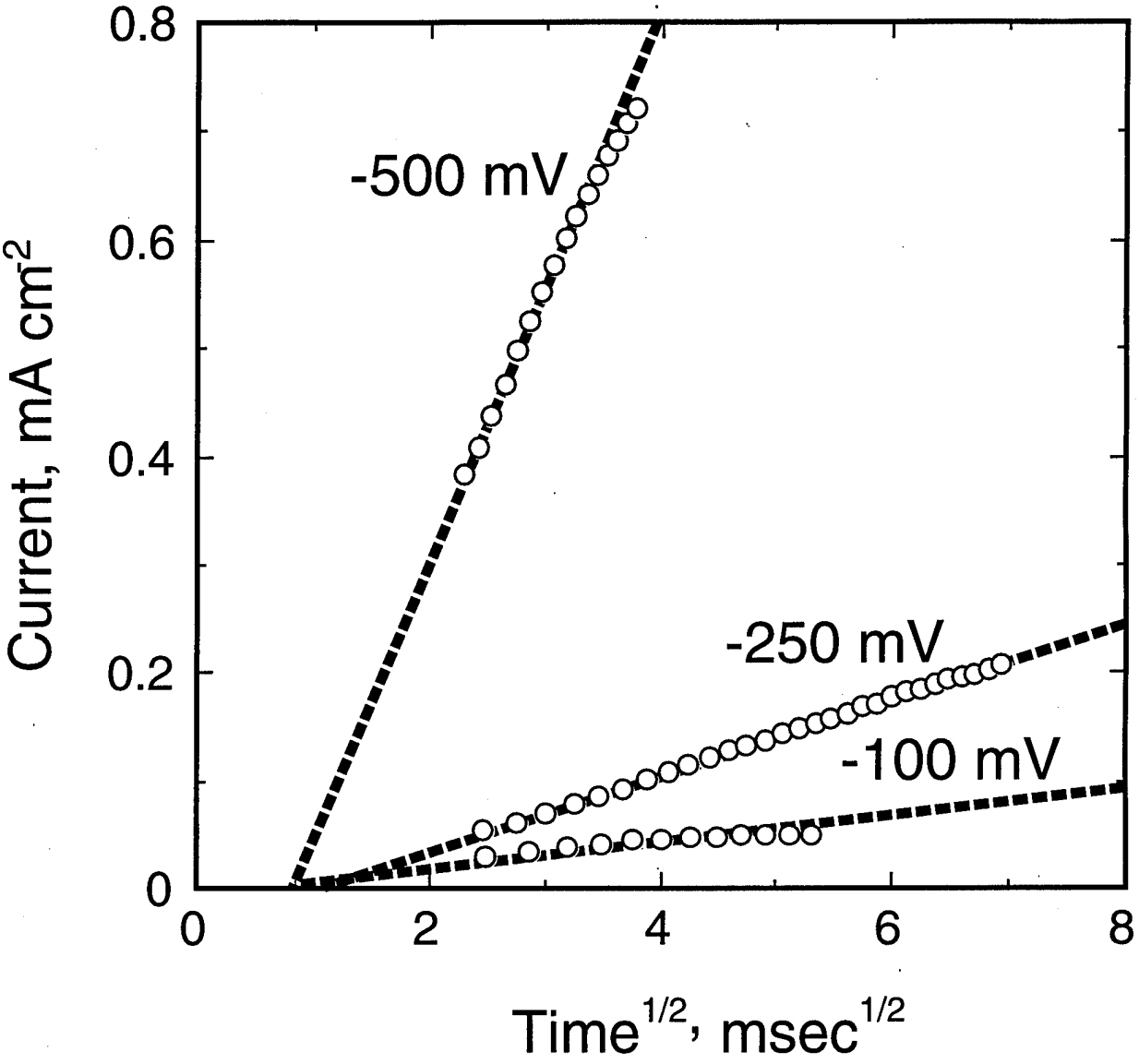

Figure 2B. Zoval *et al.*, **UCI Chemistry**

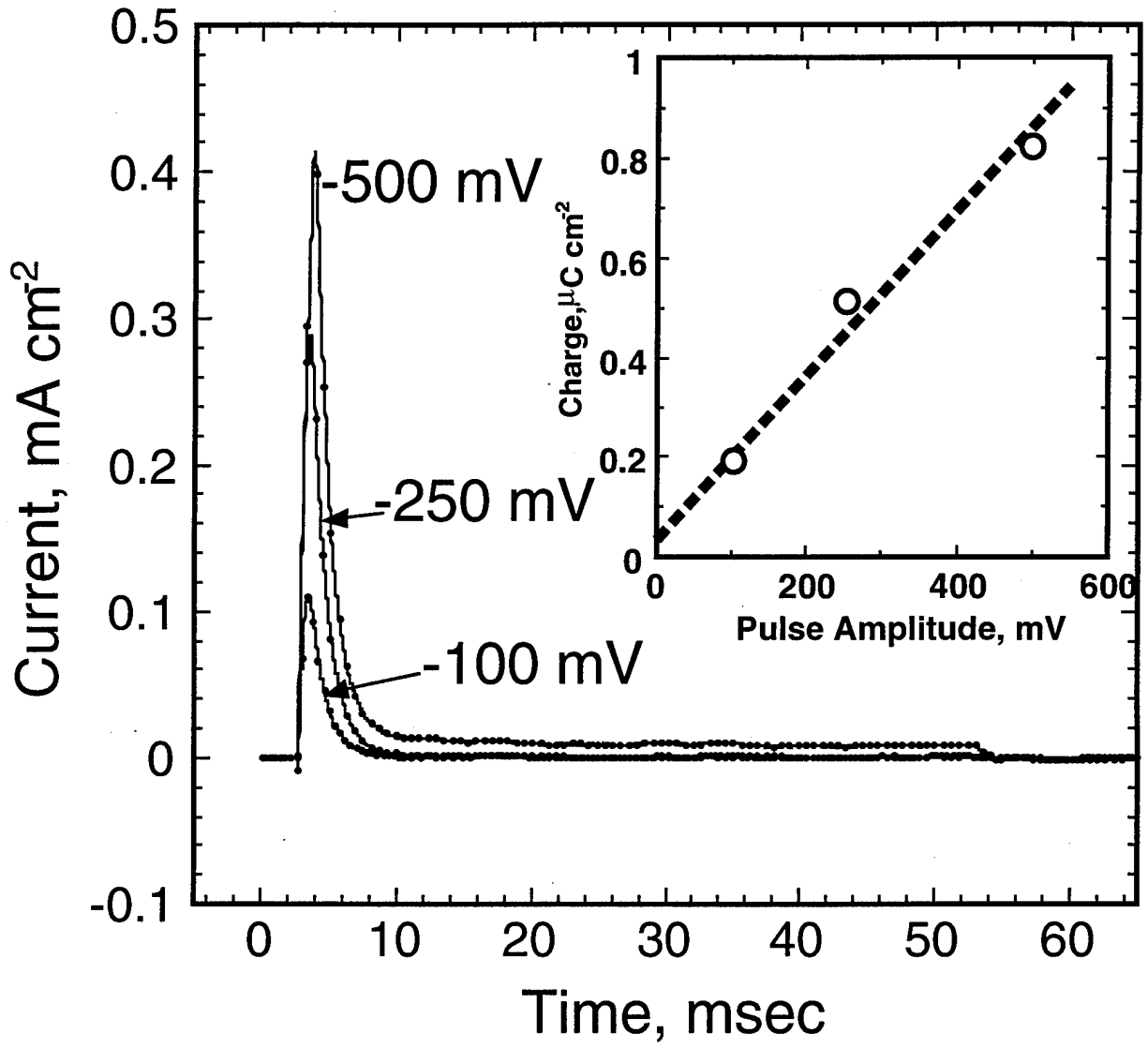

Figure 3. Zoval *et al.*, **UCI Chemistry**

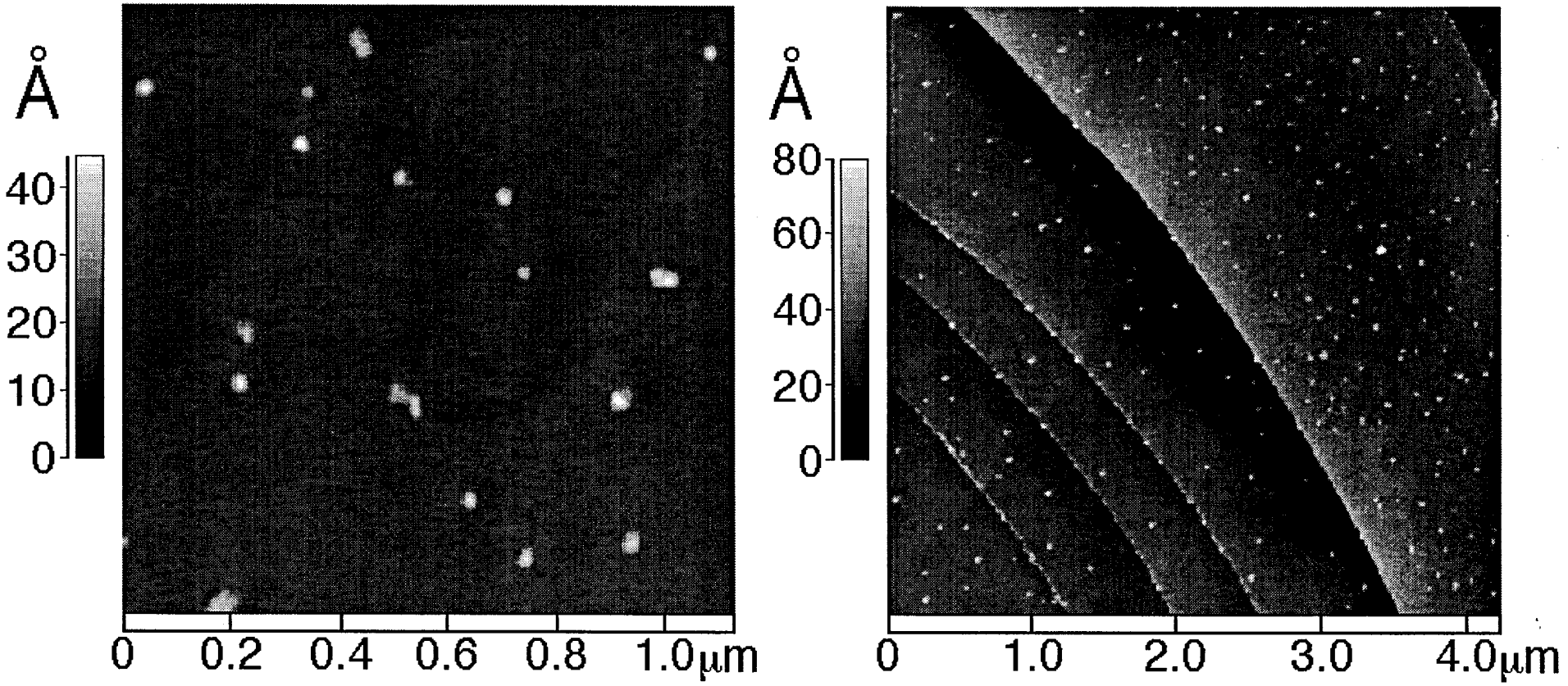

Figure 4A (left) and B. Zoval *et al.*, **UCI Chemistry**

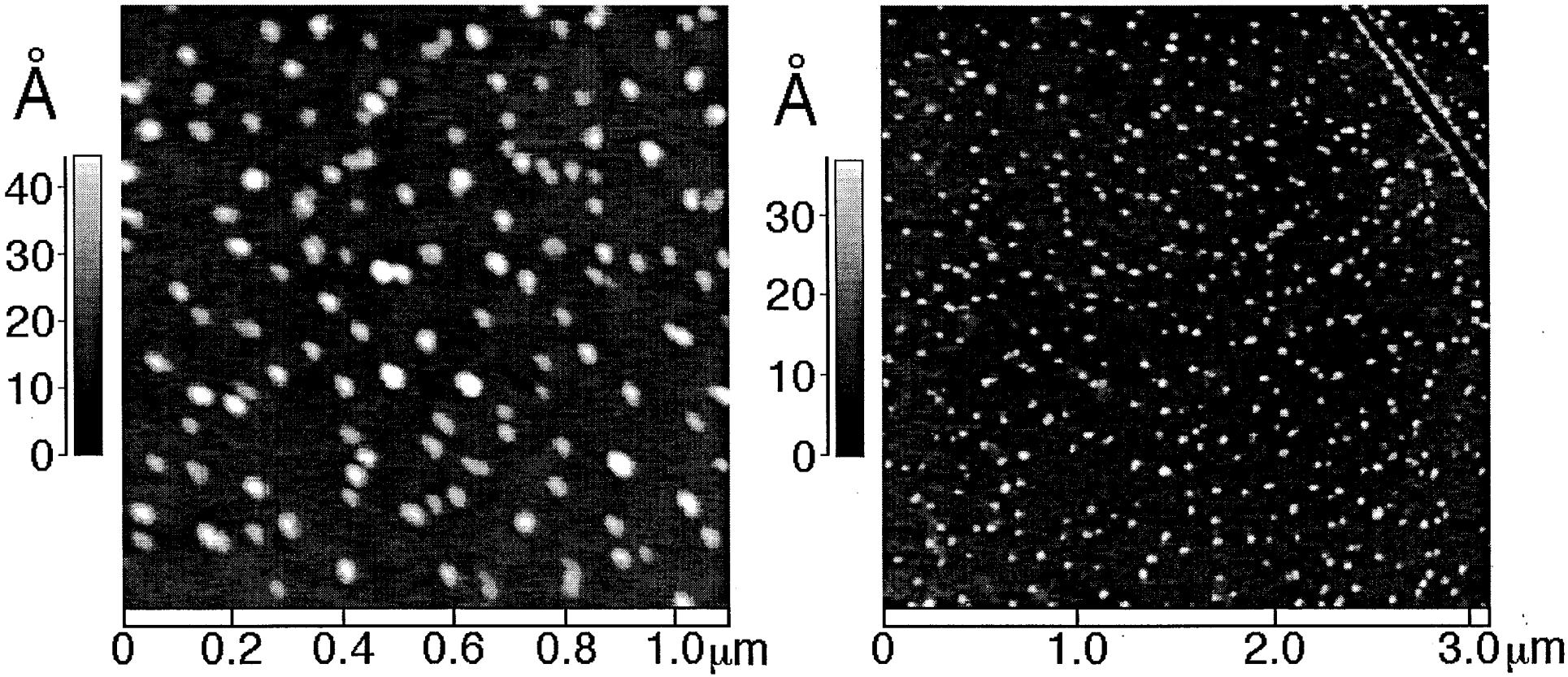

Figure 4C (left) and D. Zoval *et al.*, **UCI Chemistry**

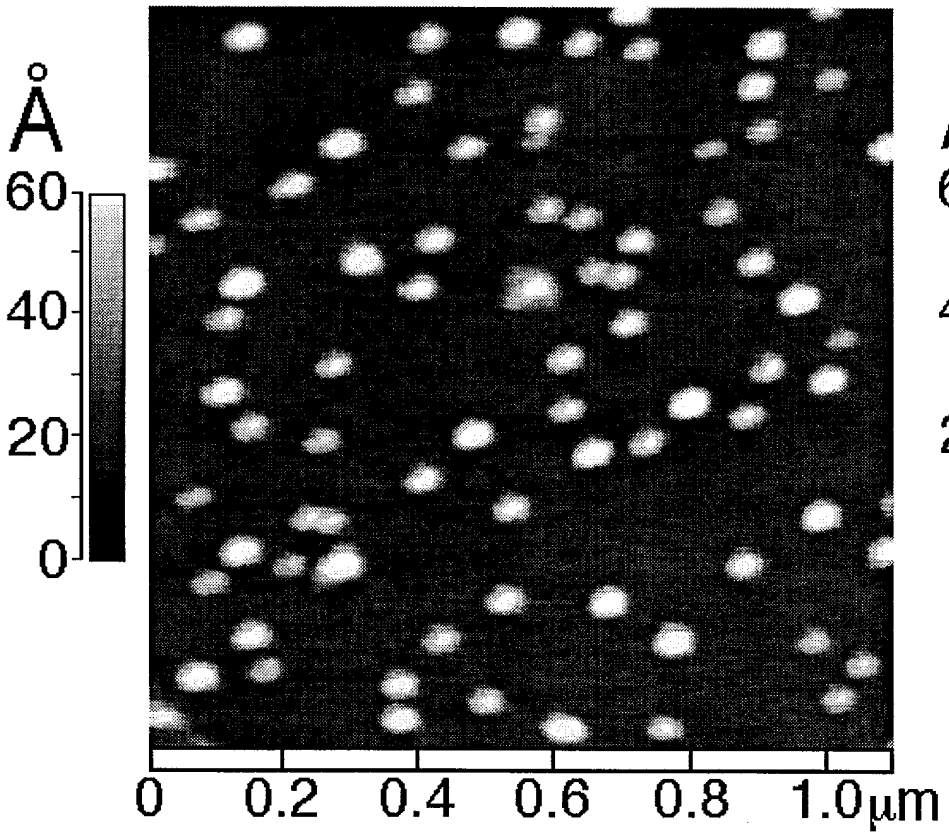

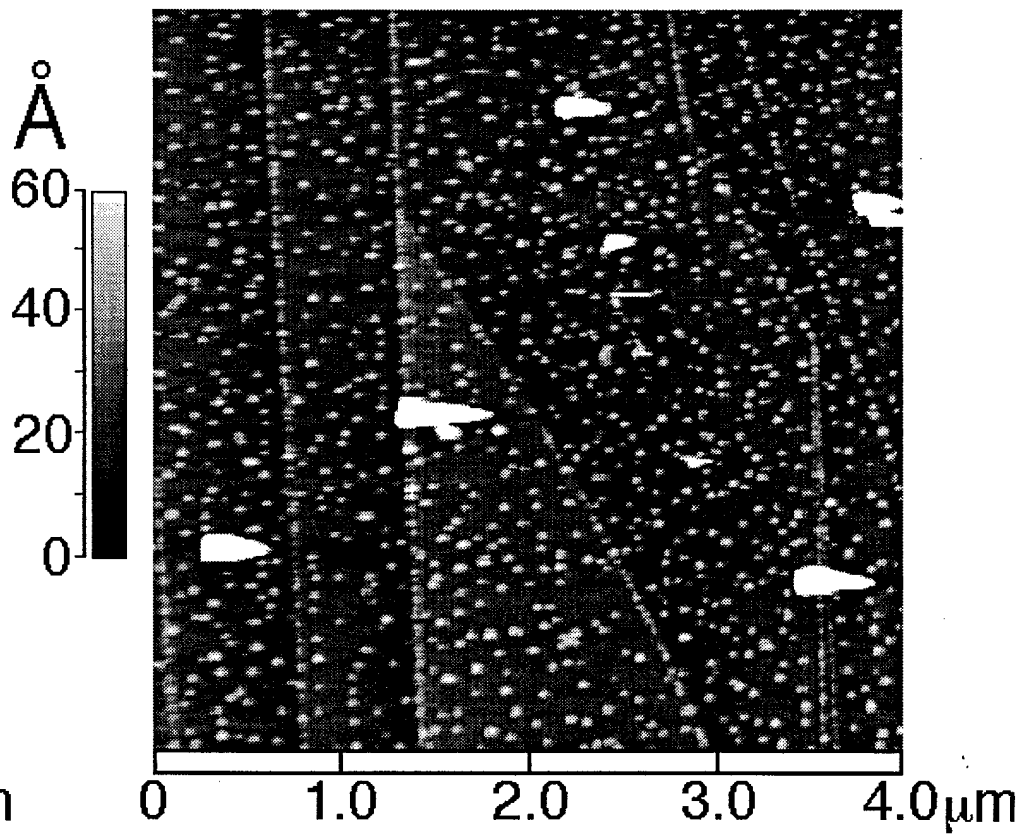

Figure 4E (left) and 4F. Zoval *et al.*, **UCI Chemistry**

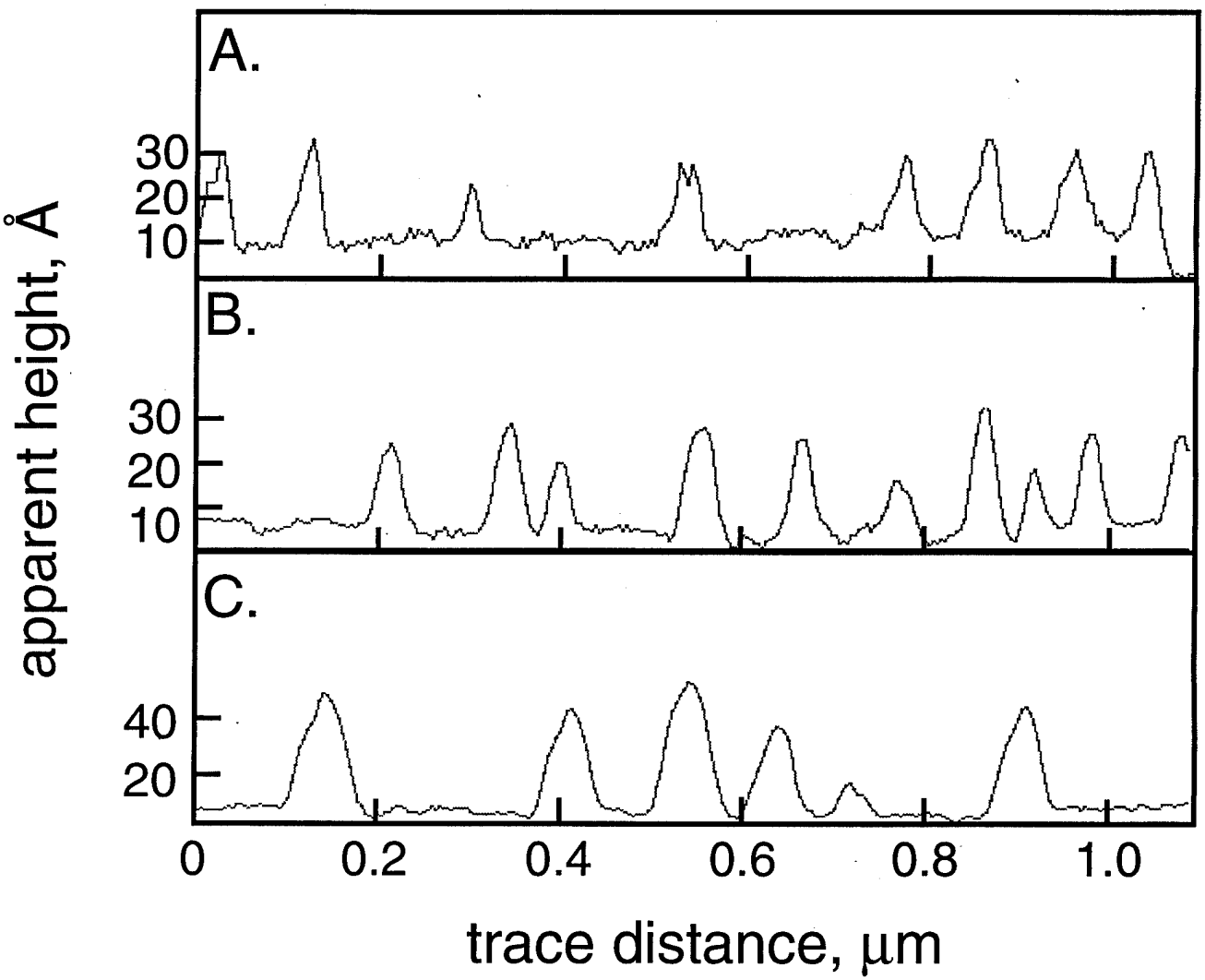

Figure 5. Zoval *et al.*, **UCI Chemistry**

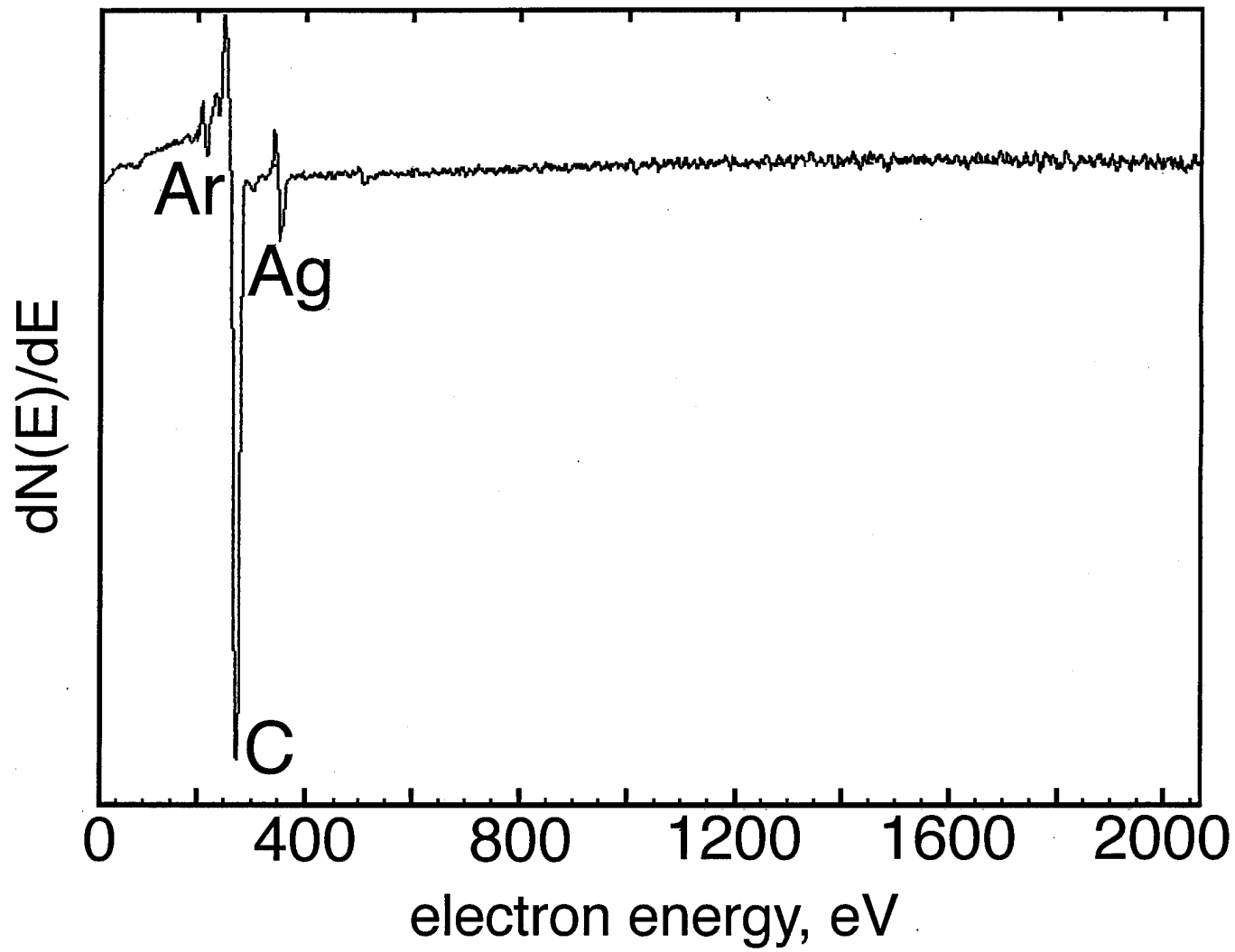
Ar
Ag
C
dN(E)/dE
0
400
800
1200
1600
2000
electron energy, eV

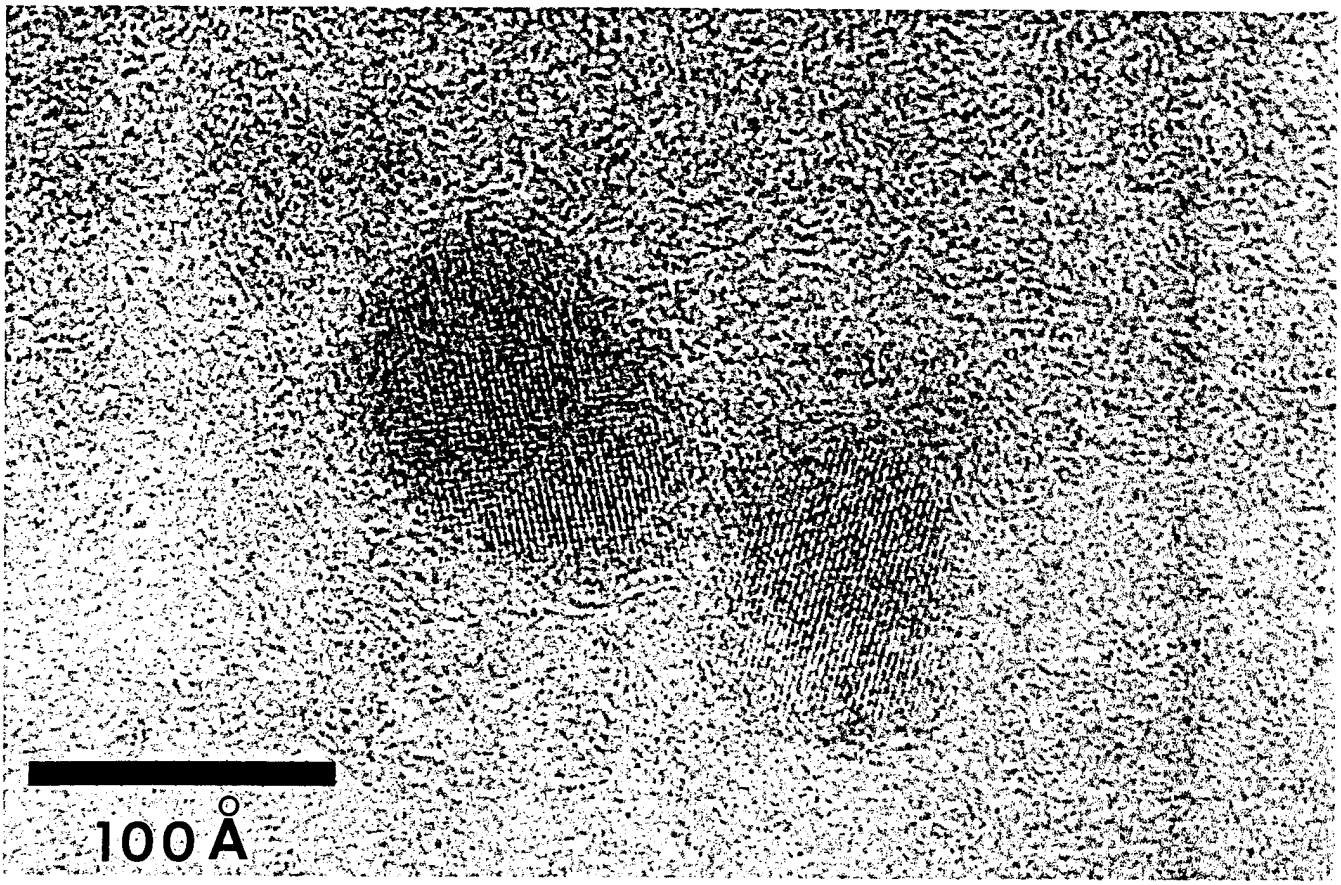
100 Å

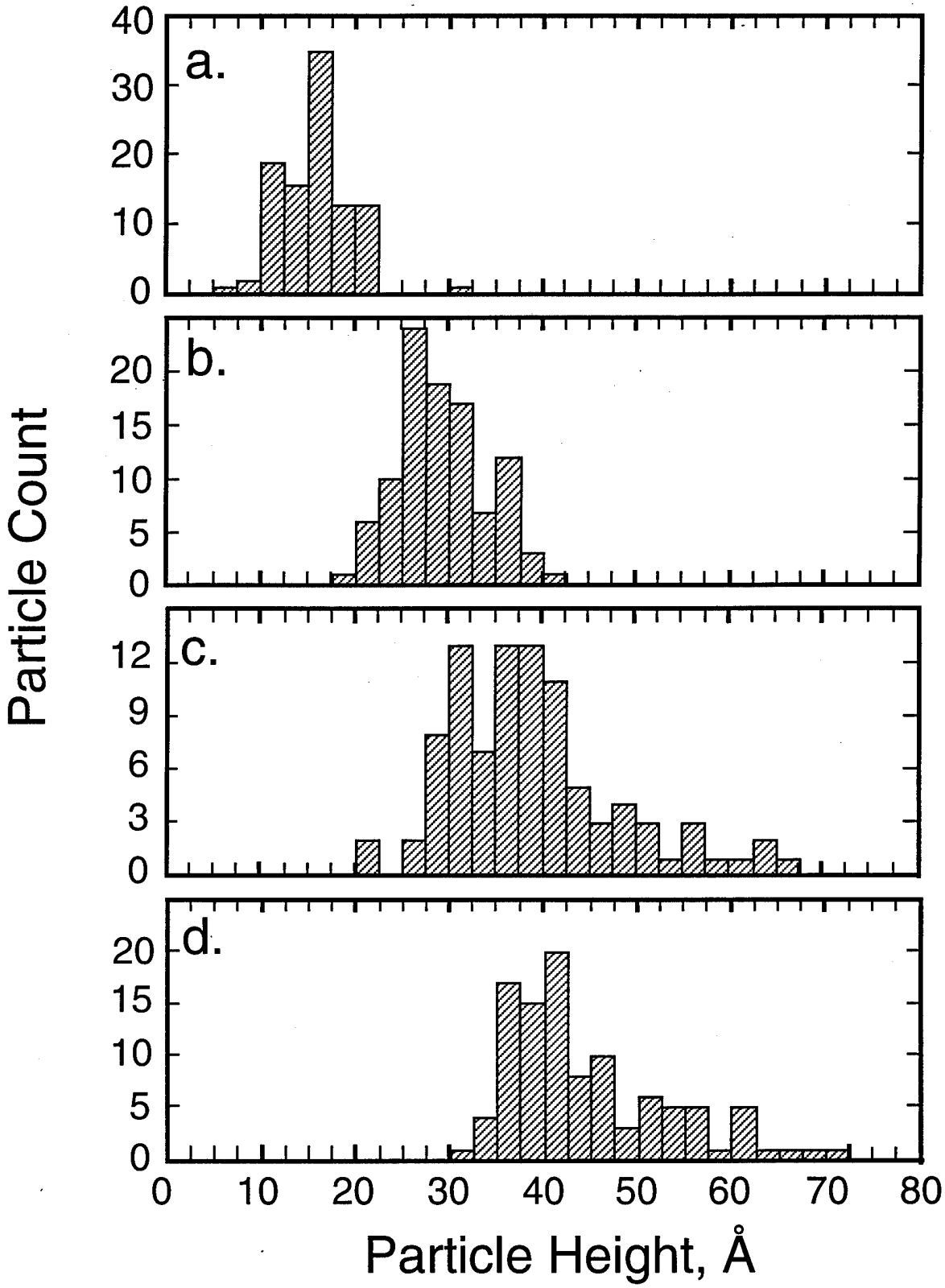

Figure 8A. Zoval *et al.*, **UCI Chemistry**

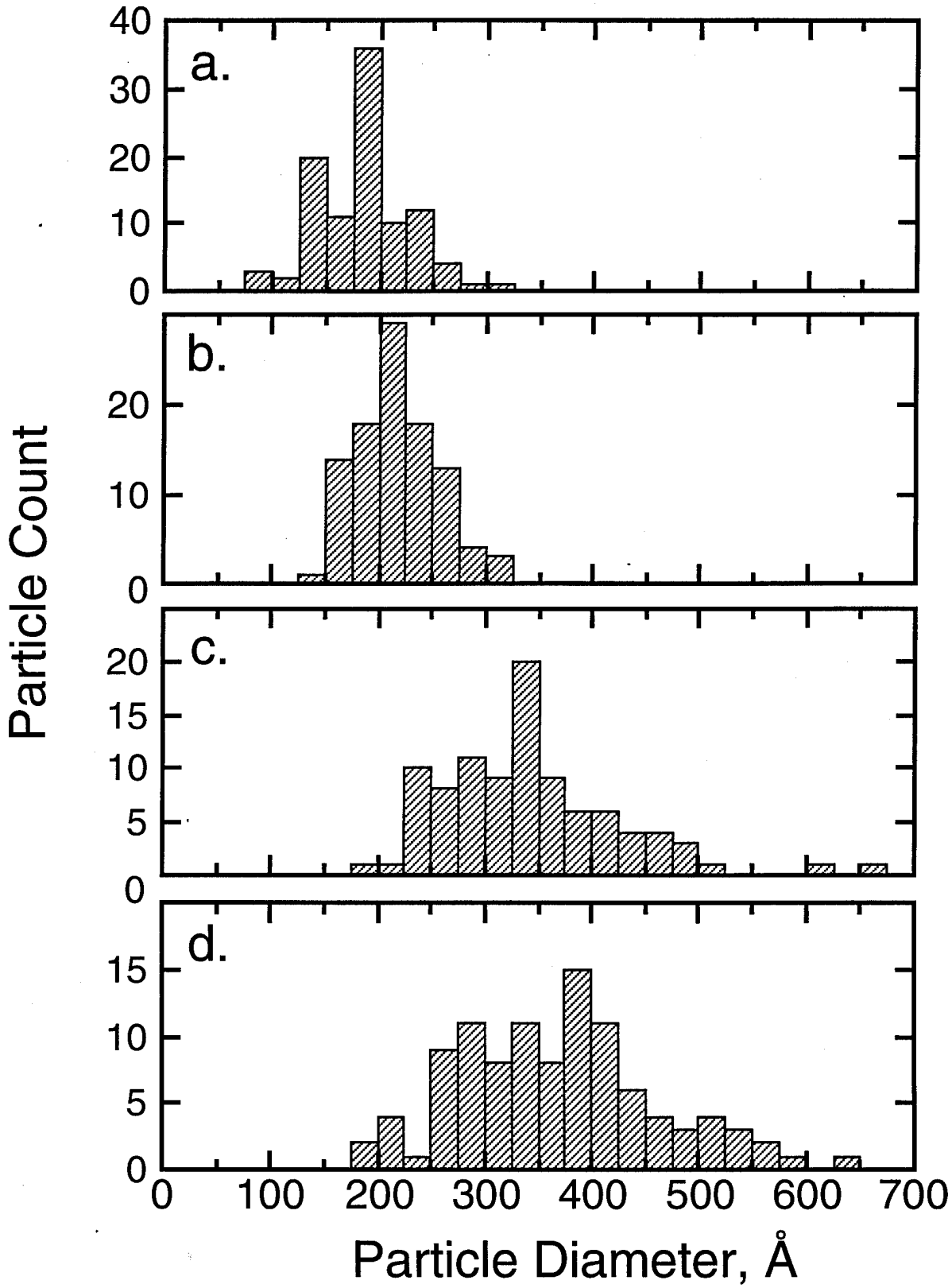

Figure 8B. Zoval *et al.*, **UCI Chemistry**

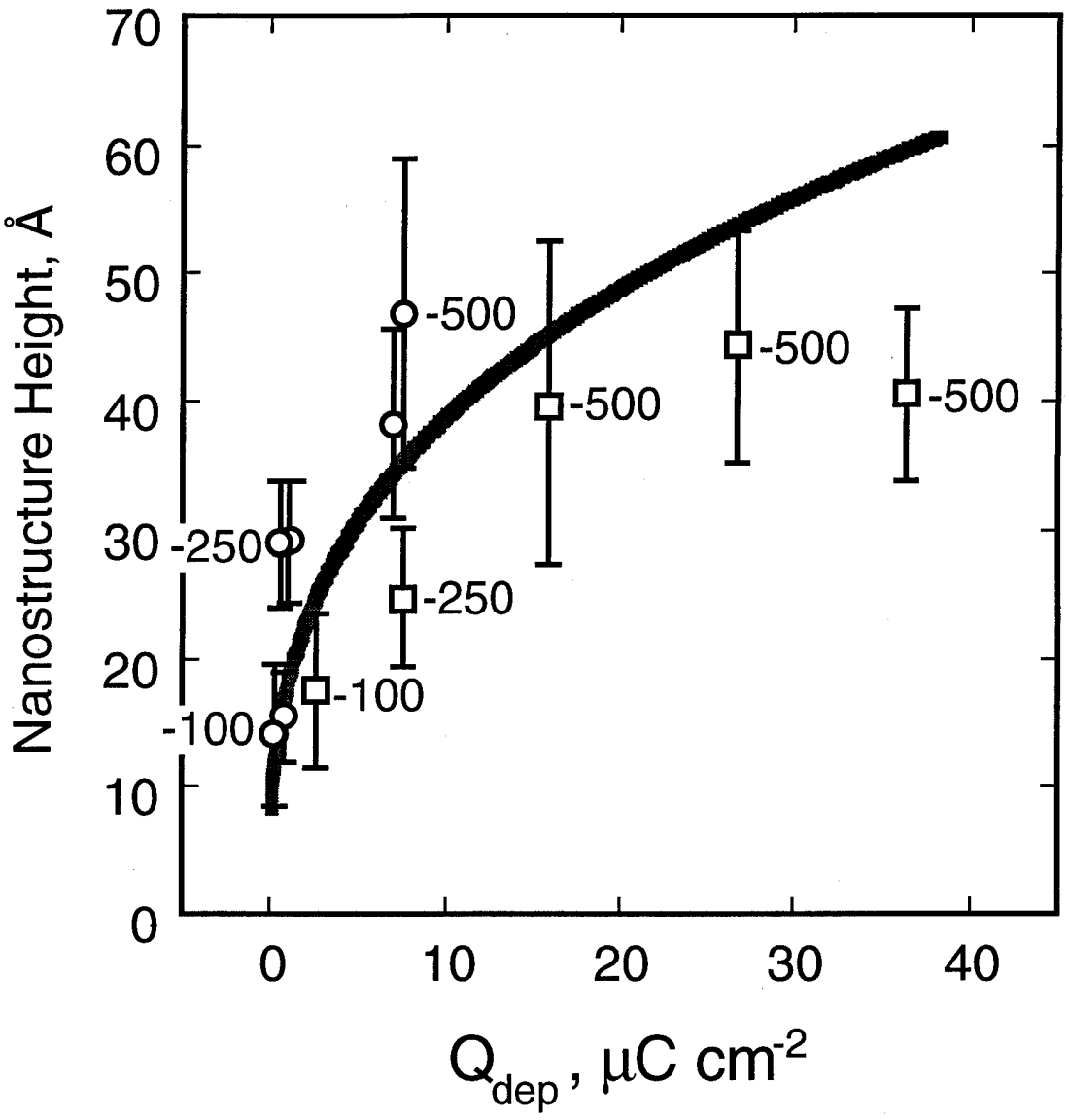

Figure 9. Zoval *et al.*, **UCI Chemistry**